



This is a repository copy of *Effect of SR-microCT radiation on the mechanical integrity of trabecular bone using in situ mechanical testing and digital volume correlation*.

White Rose Research Online URL for this paper:  
<http://eprints.whiterose.ac.uk/138611/>

Version: Accepted Version

---

**Article:**

Fernandez, M.P., Cipiccia, S., Dall'Ara, E. [orcid.org/0000-0003-1471-5077](https://orcid.org/0000-0003-1471-5077) et al. (6 more authors) (2018) Effect of SR-microCT radiation on the mechanical integrity of trabecular bone using in situ mechanical testing and digital volume correlation. *Journal of the Mechanical Behavior of Biomedical Materials*, 88. pp. 109-119. ISSN 1751-6161

<https://doi.org/10.1016/j.jmbbm.2018.08.012>

---

Article available under the terms of the CC-BY-NC-ND licence  
(<https://creativecommons.org/licenses/by-nc-nd/4.0/>).

**Reuse**

This article is distributed under the terms of the Creative Commons Attribution-NonCommercial-NoDerivs (CC BY-NC-ND) licence. This licence only allows you to download this work and share it with others as long as you credit the authors, but you can't change the article in any way or use it commercially. More information and the full terms of the licence here: <https://creativecommons.org/licenses/>

**Takedown**

If you consider content in White Rose Research Online to be in breach of UK law, please notify us by emailing [eprints@whiterose.ac.uk](mailto:eprints@whiterose.ac.uk) including the URL of the record and the reason for the withdrawal request.



[eprints@whiterose.ac.uk](mailto:eprints@whiterose.ac.uk)  
<https://eprints.whiterose.ac.uk/>

# Effect of SR-microCT radiation on the mechanical integrity of trabecular bone using *in situ* mechanical testing and digital volume correlation

Marta Peña Fernández<sup>1</sup>, Silvia Cipiccia<sup>2</sup>, Enrico Dall'Ara<sup>3</sup>, Andrew J Bodey<sup>2</sup>, Rachna Parwani<sup>1</sup>, Martino Pani<sup>1</sup>, Gordon W Blunn<sup>4</sup>, Asa H Barber<sup>1,5</sup>, Gianluca Tozzi<sup>1\*</sup>

## Affiliations:

1. Zeiss Global Centre, School of Engineering, University of Portsmouth, Portsmouth, UK.
2. Diamond Light Source, Oxfordshire, OX11 0QX, UK.
3. Department of Oncology and Metabolism and INSIGNEO institute for in silico medicine, University of Sheffield, Sheffield, UK.
4. School of Pharmacy and Biomedical Sciences, University of Portsmouth, Portsmouth, UK.
5. School of Engineering, London South Bank University, London, UK,

## \*Corresponding author:

Dr. Gianluca Tozzi  
Zeiss Global Centre  
School of Engineering  
University of Portsmouth  
Anglesea Building, Anglesea Road  
PO1 3DJ, Portsmouth  
United Kingdom  
Tel: +44 (0)239284 2514  
Email: [gianluca.tozzi@port.ac.uk](mailto:gianluca.tozzi@port.ac.uk)

## Word count

Abstract: 207 words  
Introduction-Conclusion: 5566 words  
Tables: 2  
Figures: 8  
Supplementary data: 2

## **ABSTRACT**

The use of synchrotron radiation micro-computed tomography (SR-microCT) is becoming increasingly popular for studying the relationship between microstructure and bone mechanics subjected to in situ mechanical testing. However, it is well known that the effect of SR X-ray radiation can considerably alter the mechanical properties of bone tissue. Digital volume correlation (DVC) has been extensively used to compute full-field strain distributions in bone specimens subjected to step-wise mechanical loading, but tissue damage from sequential SR-microCT scans has not been previously addressed. Therefore, the aim of this study is to examine the influence of SR irradiation-induced microdamage on the apparent elastic properties of trabecular bone using DVC applied to in situ SR-microCT tomograms obtained with different exposure times. Results showed how DVC was able to identify high local strain levels ( $>10,000 \mu\epsilon$ ) corresponding to visible microcracks at high irradiation doses ( $\sim 230$  kGy), despite the apparent elastic properties remained unaltered. Microcracks were not detected and bone plasticity was preserved for low irradiation doses ( $\sim 33$  kGy), although image quality and consequently, DVC performance were reduced. DVC results suggested some local deterioration of tissue that might have resulted from mechanical strain concentration further enhanced by some level of local irradiation even for low accumulated dose.

### **Keywords:**

Bone; X-ray radiation; dose; tissue damage; SR-microCT; digital volume correlation; in situ testing.

## 1. Introduction

A deep understanding of bone mechanics at different dimensional scales is of fundamental importance since musculoskeletal pathologies such as osteoporosis or bone metastasis are associated with alterations in the bone structure [1]. Thus, advances in mechanical characterisation of bone at the micro- and nanoscale [2–4] would ultimately improve the assessment of the effect of treatments and interventions in pathological conditions [5,6].

Several studies have investigated the relationship between microstructure and bone tissue mechanics using a combination of mechanical testing and X-ray micro-computed tomography (microCT), known as in situ (or 4D) microCT [7–10]. However, in situ experiments performed in laboratory microCT systems require long times to acquire high quality tomograms (high signal to noise ratio (SNR)) and reducing the scanning time is therefore an essential requirement. In this perspective, high-energy synchrotron radiation micro-computed tomography (SR-microCT) has become a very powerful technique able to combine fast acquisition of three-dimensional (3D) microstructures with high spatial resolution ( $\sim 1 \mu\text{m}$  voxel size) [11,12]. Over the past decade, SR-microCT was employed for studying the microarchitecture and deformation field of bone under in situ mechanical testing [13–15], notably enhancing the understanding of bone failure mechanisms. Unfortunately, the cumulative effect of sequential step-wise SR-microCT irradiation on the mechanical properties of bone tissue was never addressed.

Important guidelines to date on the effect of X-ray irradiation on bone mechanics were described in Barth et al. [16,17] who reported how high exposures to SR X-ray radiation lead to a deterioration of the mechanical properties of bone resulting in reduced strength, ductility and toughness as a consequence of collagen matrix degradation. Particularly, in [16, 17] deformation and fracture of human cortical bone were evaluated following irradiations up to 630 kGrays (kGy) to simulate typical scan time for a tomographic data set. It was shown how plastic deformation was suppressed after 70 kGy of radiation, due to the reduction of strain carried by the collagen fibrils from  $\sim 80\%$  (unirradiated) to  $\sim 40\%$  of the applied tissue strain, and apparent strain decreased by a factor of five after tripling the radiation dose; ultimately, suggesting that in situ SR-microCT testing, typically requiring multiple sequential tomograms of the same sample over time, may result in accumulation of significantly large radiation doses that affect mechanical properties [6]. However, despite an ideal safety value in the region of 35 kGy (and below) was suggested, corresponding to the typical dose used to sterilize bone allografts [18], uncertainties still remain on what is the effect of X-ray SR radiation on the genesis and development of bone microdamage with different accumulated dose. Particularly, the impact of the total radiation dose, close to the proposed limit of 35 kGy, on bone elastic properties. In addition, dose calculation on bone in Barth et al. [16, 17] was carried out on mathematical terms taking into account only bone mass and assuming a reasonably uniform distribution for the absorption of X-rays within the sample. This may be working well in some experiments but not in others where multiple materials are on the beam-path (i.e. in situ loading devices containing the bone in saline solution) and certainly can only provide an average evaluation, where local dose on the tissue cannot be estimated.

With the recent and rapid advances of high-resolution microCT in conjunction with in situ mechanical testing [19,20], digital volume correlation (DVC) [21] has gained increasing popularity as the only image-

based experimental technique capable of investigating 3D full-field displacement and strain in trabecular bone [22–25], cortical bone [25,26], whole bones [27–30], biomaterials [31] and bone-biomaterial systems [32] under different loading conditions. Very recently, DVC applied to SR-microCT of bone has been used to characterise the level of uncertainties in displacement and strain measurements for different bone types, including bovine trabecular, bovine cortical and murine tibiae [33]. However, to the authors knowledge, there is only one study using DVC for actual in situ SR-microCT testing of cortical bone [26], but none reporting SR-microCT-based DVC for trabecular bone. In addition, Christen et al. [26] proposed a DVC analysis, assuming that the obtained displacements and strains were only related to the bone mechanics and virtually ‘unaffected’ by the SR radiation and total accumulated radiation dose during sequential tomography. Therefore, it is critical to evaluate how bone mechanics, particularly in the elastic regime, is influenced by SR-microCT exposure during in situ experiments on bone, confirming that the irradiation does not induce important damage to the tissue. This is also a mandatory pre-requisite to fully enable the application of DVC computed on bone undergoing in situ SR-microCT mechanical testing, particularly for tomograms with resulting quality that may be limited by safe X-ray dose. On the other hand, the unique ability of DVC to detect local levels of strains in bone structures with the consequent possibility of predicting failure location [30] when values in the range of 8,000-10,000  $\mu\epsilon$  (deemed sufficient to produce bone tissue yielding [34,35]) are computed can provide precious indications on the local degree of tissue deterioration due to cumulative SR X-ray exposure.

The aim of this study was therefore to use DVC applied to in situ SR-microCT images of trabecular bone in order to investigate, for the first time, the influence of SR irradiation-induced tissue damage on the apparent elastic properties at variable radiation doses. In addition, the dose distribution delivered to bone specimens was simulated to gain a better understanding on the combination of local irradiation and mechanical strain concentration on tissue damage. Doses ranging from 4.7 to 32.9 kGy per tomogram were investigated, achieved by varying the exposure time to SR X-ray radiation (from 64 to 512 ms per projection). The findings of this paper will improve knowledge on bone degradation during SR X-ray exposure and provide important indications on procedures to be used for in situ mechanics and DVC evaluation.

## **2. Methods**

### **2.1. Specimen preparation**

Ovine trabecular bone from fresh frozen femoral condyles was used in this study, following Ethics approval granted by the Royal Veterinary College and in compliance with the United Kingdom Home Office regulations (Animal Scientific Procedures Act [1986]). Four cylindrical cores, 18 mm in height, 4 mm in diameter were extracted from the femoral lateral condyles in proximal-distal direction by drilling with a coring tool and the ends of the cores were trimmed plane and parallel. End-constraint was achieved by embedding the ends of the samples in poly-methyl-methacrylate (PMMA) endcaps. Approximately, 5 mm of bone was embedded into each endcap to achieve a 2:1 aspect ratio and reduce experimental artifacts [36]. Samples were kept frozen at  $-20^{\circ}$  and thawed for approximately 2h in saline solution at room temperature before testing.

## 2.2. SR-microCT imaging and in situ mechanics

SR-microCT was performed at the Diamond-Manchester Imaging Branchline I13-2 [37] of Diamond Light Source (DLS), UK. A filtered (1.3 mm pyrolytic graphite, 3.2 mm aluminium and 60  $\mu\text{m}$  steel) polychromatic 'pink' beam (5-35 keV) was used with an undulator gap of 5 mm for data collection and, to limit sample damage, 11 mm for low-dose alignment. The propagation (sample-to-scintillator) distance was approximately 50 mm. Images were recorded by a pco.edge 5.5 (PCO AG, Germany) detector which was coupled to a 500  $\mu\text{m}$ -thick  $\text{CdWO}_4$  scintillator and a visual light microscope (Fig. 1-I). The effective voxel size was 2.6  $\mu\text{m}$ , with a field of view of 6.7 x 5.6 mm. Different X-ray radiation doses were obtained for each specimen by using variable exposure times per projection: 512, 256, 128 and 64 ms, with 11 ms overhead per exposure. For each dataset, 1801 projection images were collected over 180 degrees of continuous rotation ('fly scan'). The final image was not used for reconstruction but was compared to the first image to check for experimental problems including sample deformation and bulk movements [38]. The projection images were flat and dark corrected prior to reconstruction. For each dataset, 40 flat and dark images were collected. Reconstruction was performed at DLS using the in-house software, DAWN [38,39], incorporating ring artefact suppression.

In situ uniaxial compression testing was performed via a micro-mechanical loading stage (CT5000, Deben Ltd, UK). Specimens were immersed in saline solution throughout the test to simulate physiological conditions. All tests were carried out under displacement control at a constant cross-head speed of 0.1 mm/min. A small preload (5 N) was first applied to ensure good end contact prior to testing, followed by 10 cycles of preconditioning. Each bone specimen was then subjected to seven loading cycles in the apparent elastic range [39] (0.5% global strain) and full tomographic datasets were acquired under compression at the end of each cycle (Figure 2), after allowing the samples to settle for 10 minutes to reduce stress relaxation during imaging. Specimens that did not show any visible microdamage (i.e. microcracks) after visual inspection of the reconstructed images at the end of the loading cycles were loaded up to failure to investigate the presence of apparent plasticity in the bone. For each specimen, seven datasets were obtained corresponding to the different loading cycles. The 3D images (Figure 1-II, III) were filtered (Figure 1-IV) and masked (Figure 1-V) prior to DVC analysis (Supplementary Material S1). Additionally, the bone volume (BV) was obtained using BoneJ [40] plugin for Fiji to assess possible correlations with DVC measurements.

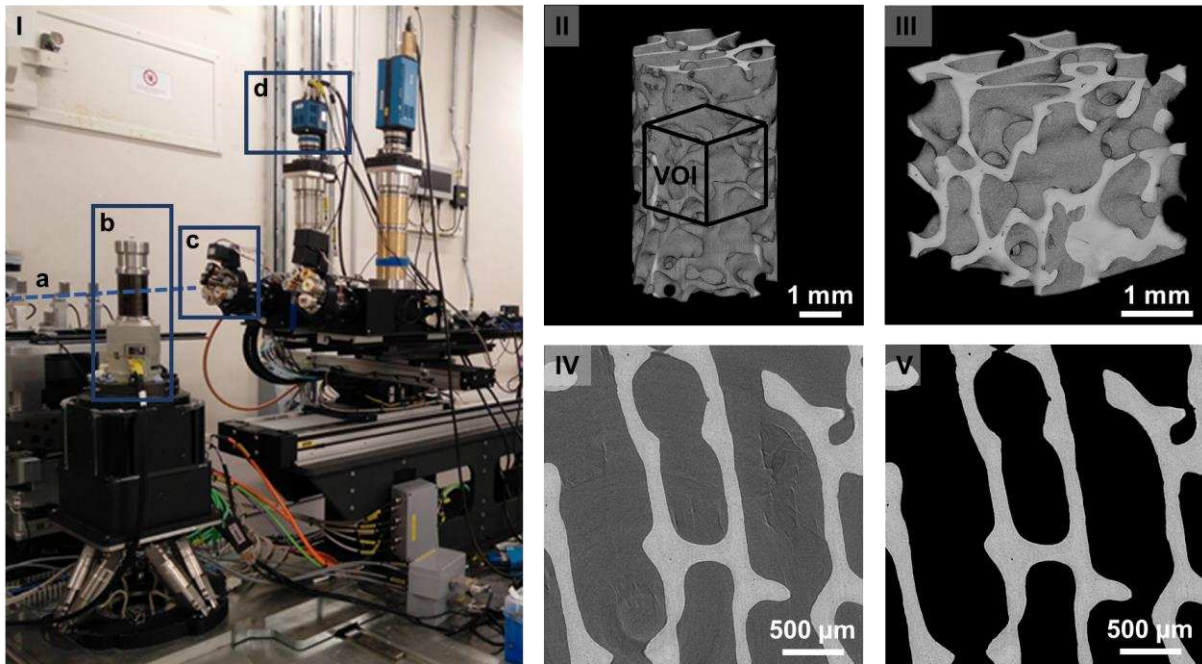


**Figure 1.** (I) Experimental setup at I13-2 beamline. The direction of the beam is indicated by the dashed line (a). Samples were scanned within the loading stage (b) using a pco.edge 5.5 detector (c) and a 1.25X objective (2.5X total magnification) (d). SR-microCT reconstruction of trabecular bone (II): each cylindrical specimen was imaged with an effective voxel size of 2.6  $\mu\text{m}$  using different exposure times: 512, 256, 128 and 64 ms. A cubic (1000\*1000\*1000 voxels) volume of interest (VOI) was obtained at the centre of each specimen (III). 2-dimensional (2D) slice through the middle of the VOI before (IV) and after (V) mineralised tissue was masked from the marrow.

### 2.3. Dose calculation

The average photon energy and photon flux during the synchrotron experiment was estimated using SPECTRA code [41], to be 28.93 keV and  $4.9 \times 10^{13}$  photons/s respectively (23 keV and  $3 \times 10^{10}$  photons/s during alignment), using a 2 x 2 mm aperture 220 m after the X-ray source. These values took in consideration the transmission of the filters and the reflectivity of the platinum mirror used during the experiment. The delivered dose rate was simulated using FLUKA Monte Carlo code [42], for the fixed set of parameters used in the Beamline. The geometry simulated in FLUKA consisted on a trabecular bone specimen within the loading device (Supplementary Material S2). The bone specimen was assumed as a cylinder (4 mm diameter, 10 mm length, density of 0.5 g/cm<sup>3</sup> [43]) placed in the centre of the environmental chamber (40 mm inner diameter, 3 mm thickness) made of glassy-carbon (density of 1.5 g/cm<sup>3</sup>) and filled with saline solution (density of 1 g/cm<sup>3</sup>). The chamber was located inside the loading stage glassy-carbon tube (56 mm inner diameter, 4.5 mm thickness). The implemented stoichiometry was the following: Ca-22.5, P-10.3, C-15.5, N-4.2, O-43.5, S-0.3, Mg-0.2. The simulation results have an error below 15%. Further details on the dose simulation can be found on the Supplementary Material S2. The nominal radiation dose absorbed by each sample during sequential tomography was computed multiplying the dose rate by the scanning time (Table 1).

### 2.4. Digital volume correlation

DaVis-DC software (v8.3, LaVision, Goettingen, Germany) was used to couple SR irradiation-induced damage and mechanical bone yielding with the differences in full-field strains developed in the tissue

after each loading cycle for the highly- and lowly-irradiated specimens (32.9 and 4.7 kGy/tomogram). The software is based on a local approach of DVC computation, which has been deemed sufficiently precise to be used in bone mechanics [24,32,44–47]. Details on the computation algorithm used in DaVis-DC are reported elsewhere [31,44]. The evaluation of the level of uncertainties or ‘baseline strains’ was performed in the first two consecutive datasets for both specimens, obtained under the same constant nominal strain, where the irradiation-induced damage was deemed as minimal (Supplementary material S1). DVC was applied to the masked images (where the non-bone was treated as a black ‘zero count’ region), to avoid large strain artefacts in regions with no pattern (i.e. saline solution, marrow). The presented DVC computation relied on a multi-pass scheme with a final sub-volume of 64 voxels, producing the best compromise between precision and spatial resolution (precision errors below 2  $\mu\text{m}$  for displacements and lower than 510  $\mu\epsilon$ ). This was then used to register the reference image (first loading cycle) with each of the remaining images after each loading cycle and computing the corresponding differential strain field (Figure 2).

To allow comparisons with previous studies, two different scalar indicators were computed for each registration: mean absolute differential strain value and standard deviation of the differential strain value, defined as the mean and standard deviation, respectively, of the average of the absolute values of the six components of strain for each sub-volume (similar to MAER and SDER [33,48]). The correlated volume (CV) was assessed as the volume where correlation was achieved. The correlated bone volume (CV/BV) was then computed dividing the CV by the BV. Data were screened for outliers applying the criterion of Peirce [49] to the CV/BV. In order to evaluate the full-field differential strain distribution in the VOIs over time in relation to the deformation induced by the SR irradiation damage, maximum and minimum principal differential strains were computed for the samples exposed to higher and lower radiation. Additionally, the damaged bone volume ( $BV_y$ ) was computed as the tissue voxels exceeding  $\pm 10,000 \mu\epsilon$ .

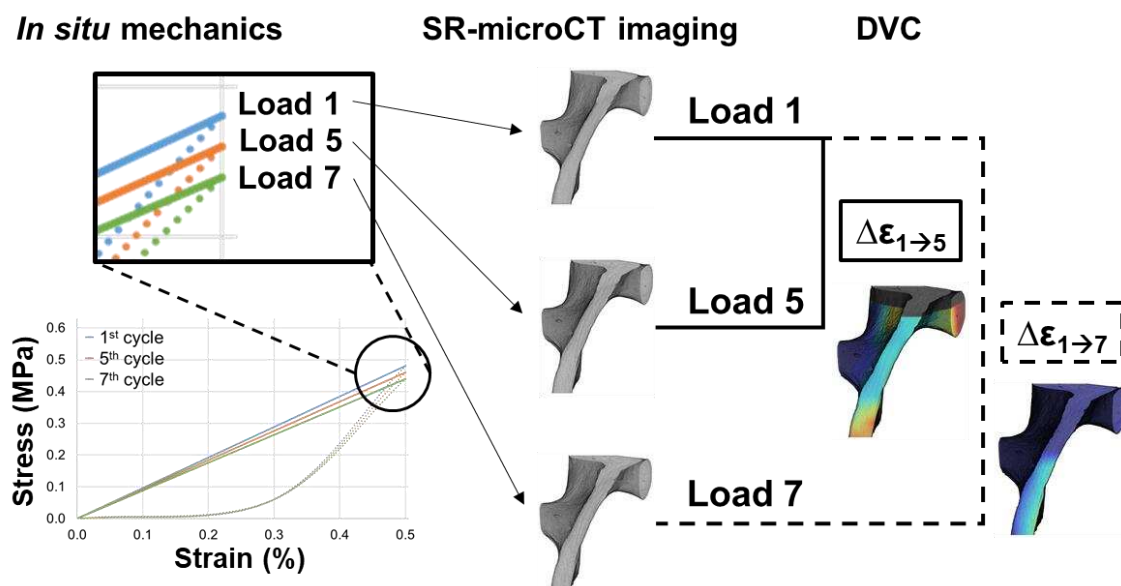


**Figure 2.** Workflow used to combine in situ SR-microCT and DVC. Specimens were cyclically loaded in the apparent elastic regime (up to 0.5% nominal strain) seven times and SR-microCT images were



acquired under maximum load. DVC was performed using the first 3D image as a reference state and computing the differential strain field between the reference and the remaining consecutive tomograms.

### 3. Results

A qualitative inspection of the SR-microCT images showed the development of multiple microcracks (Fig. 3-I, 3-II) in the samples exposed to high radiation doses (32.9 and 16.8 kGy/tomogram) that started to be visible after the fifth (164.7 kGy accumulated dose) and sixth cycles (100.9 kGy accumulated dose), respectively. Microdamage in the second one (16.8 kGy/tomogram) degenerated into a trabecular collapse. Samples imaged at lower radiation doses (8.8 and 4.7 kGy/tomogram) did not present any visible microcracks. Detailed images of a single trabecula (Fig. 3-III) allow a better comparison of the image quality, dependent on the exposure time. Bone lacunae can be identified only for the highest exposures (32.9, 16.8 kGy/tomogram). Additionally, important ring artifacts are visible in the 8.8 kGy specimen.

The stress-strain curves (Fig. 4) presented a different behaviour for each of the specimens studied. The apparent mechanics of the 32.9 kGy/tomogram sample (Fig. 4-I) remained within the elastic range even after the microcracks started to develop (after the fifth cycle). A maximum global stress of 0.4 MPa was reached at 0.5% nominal strain in the first cycle, and a progressive reduction of the stiffness was observed. The 16.8 kGy/tomogram sample reached the same maximum global stress (0.4 MPa) at 0.5% strain, however, the reduction of the stiffness after 5 cycles was considerably higher. A less pronounced reduction of stiffness was found for the 8.8 kGy/tomogram specimen (Fig. 4-III), whereas the sample imaged at lower radiation dose did not show any notable changes in the apparent elastic properties during the seven loading cycles (Fig. 4-IV). At a nominal applied strain of 0.5%, maximum global stress of 0.48 and 0.60 MPa were obtained for the 8.8 and 4.7 kGy/tomogram specimens, respectively. Samples imaged at the highest radiation doses failed within the estimated elastic range from the previous cycles (Fig. 4-V). For the 16.8 kGy/tomogram sample, a fragile failure was reached after the sixth loading cycle, when the microcracks started to be visible, under an applied load within the previously estimated elastic range. Conversely, the less irradiated samples did not reach the failure within the seven applied loading cycles, in agreement with the visual inspection of SR-microCT images. The 8.8 kGy/tomogram specimen did not present any plasticity before failing, which was then reached at ~1.7% global strain with an applied stress of 1.4 MPa. The stress-strain curve of the 4.7 kGy/tomogram specimen instead presented the typical behaviour of ductile cellular materials, such as trabecular bone. The yield was observed at 0.9% strain, resulting in a 0.99 MPa yield stress. Failure was experienced at 0.97 MPa stress and 3.9% strain.

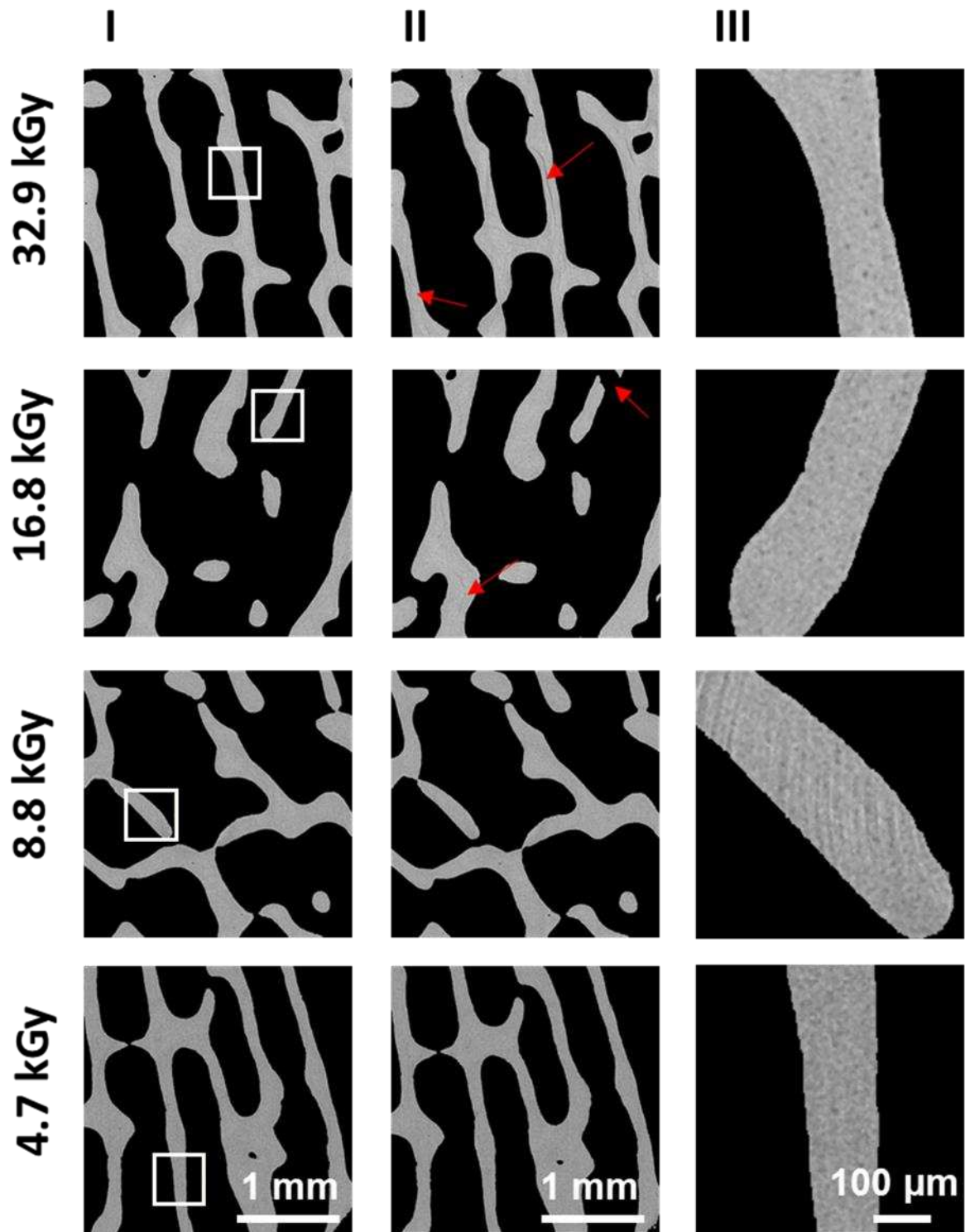


**Figure 3.** SR-microCT 2D slices acquired under load in the trabecular elastic range (0.5% apparent strain) at different radiation doses (rows for 32.9, 16.8, 8.8 and 4.7 kGy/tomogram) after the 1<sup>st</sup> (column I) and 7<sup>th</sup> (column II) loading cycles. White squares indicate regions augmented to show a single trabecula (column III). Red arrows indicate damage location in the tissue (i.e. microcrack, fracture). Bone lacunae remain visible within the trabeculae (column III) only for the highest exposures (32.9, 16.8 kGy), whereas no features could be identified for the lowest exposures (8.8, 4.7 kGy).

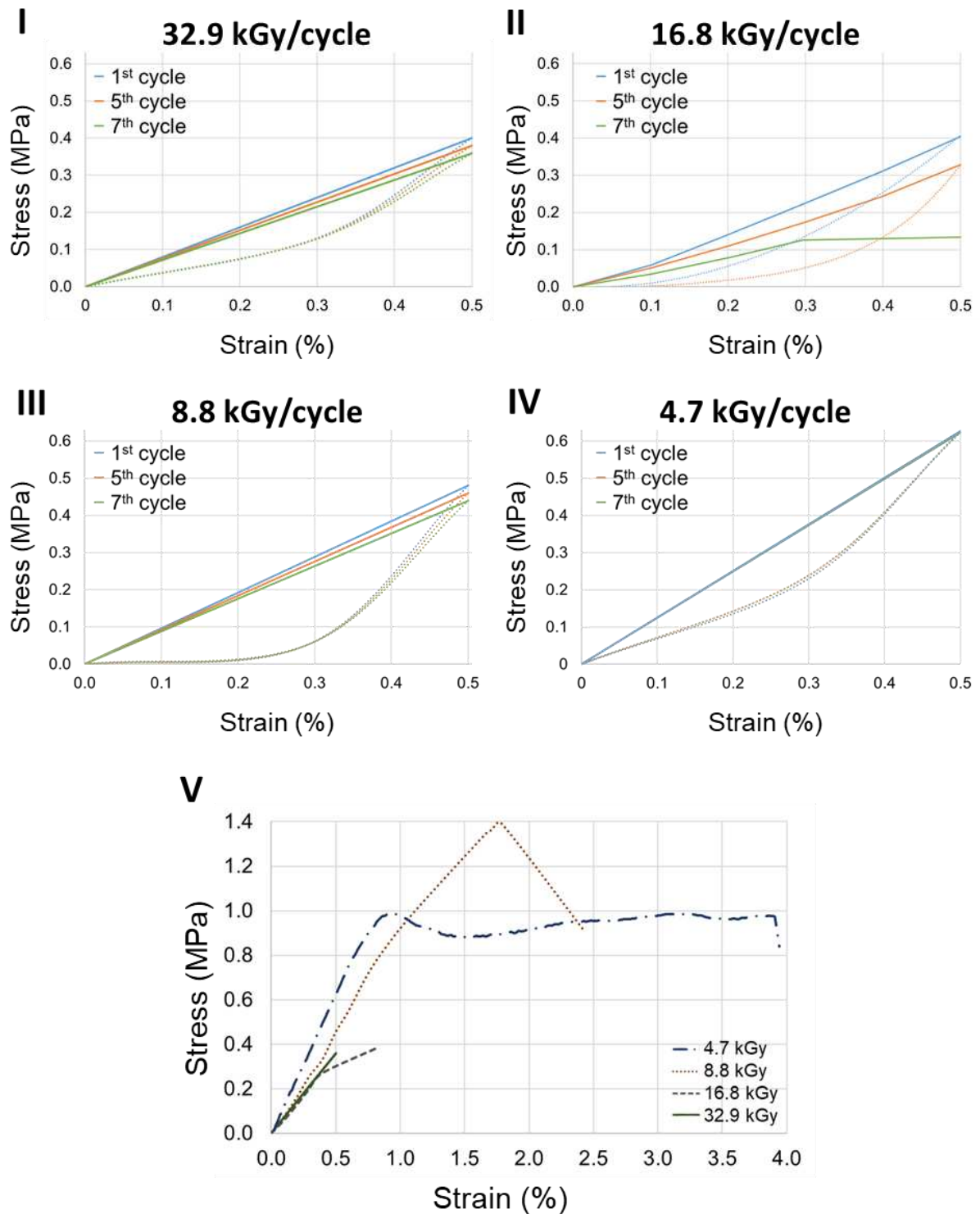


**Figure 4.** Stress-strain curves for the tested specimens. (I-IV) are showing the 1<sup>st</sup> (blue), 4<sup>th</sup> (orange) and 7<sup>th</sup> (green) loading-unloading cycles (solid-dotted curve, respectively). Reduction in the stiffness after each cycle is observed in I-III. Samples exposed to lowest doses (8.8 and 4.7 kGy/tomogram) were loaded up to failure after the seven loading cycles (V), whereas the ones at higher doses (16.8 and 32.9 kGy/tomogram) were damaged or failed within the previous seven elastic cycles.

The dose rate distribution simulated in the bone cylinder is shown in Figure 5. Maximum dose (58 Gy/s) is accumulated in the centre of the specimen (Fig. 5-II, III) where the X-ray beam impinges on and decreases through the sample (Fig. 5-I), with minimum dose (2.7Gy/s) towards the base of the cylinder. The average dose rate within the simulated cylinder was computed as 35 Gy/s (6.4 Gy/s standard deviation) during image acquisition (0.2 Gy/s during alignment). The accumulated dose for each specimen during the sequential tomograms is reported in Table 1, together with the total scan time computed as a function of the exposure time per projection.

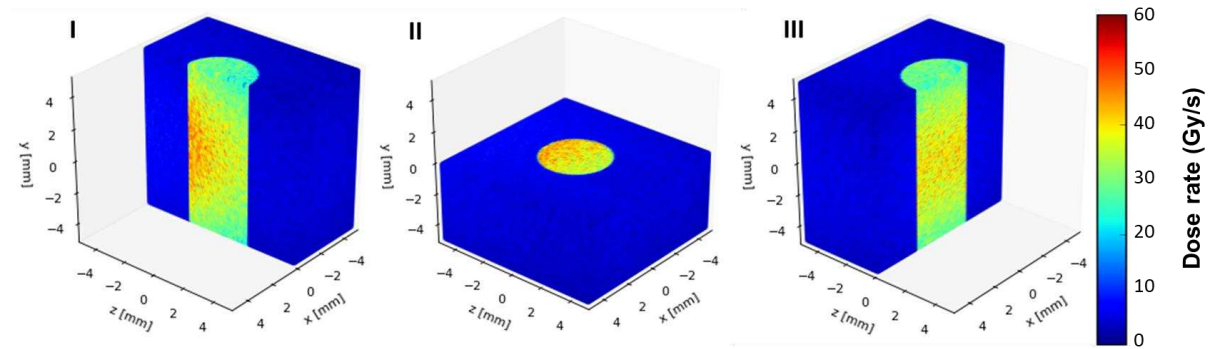


**Figure 5.** Dose rate distribution within a cylindrical trabecular bone specimen simulated in FLUKA. 3D sections in x (I), y (II) and z (III) directions of the simulated bone specimen within the saline solution are shown. The X-ray beam comes along the z direction from negative to positive direction.

**Table 1.** Total scan time and nominal radiation dose absorbed by each sample per cyclic loading, calculated by varying the exposure time. Values were truncated to one decimal place.

Exposure time	512 ms/projection						
Load cycles	1	2	3	4	5	6	7
Scan time (min)	15.7	31.4	47.1	62.8	78.5	94.1	109.8
Dose accumulated (kGy)	32.9	65.9	98.8	131.8	164.7	197.7	230.6
Exposure time	256 ms/projection						
Load cycles	1	2	3	4	5	6	7
Scan time (min)	8.0	16.0	24.0	32.0	40.1	48.1	56.1
Dose accumulated (kGy)	16.8	33.6	50.5	67.3	84.1	100.9	117.7
Exposure time	128 ms/projection						
Load cycles	1	2	3	4	5	6	7
Scan time (min)	4.2	8.3	12.5	16.7	20.9	25.0	29.2
Dose accumulated (kGy)	8.8	17.5	26.3	35.0	43.8	52.5	61.3
Exposure time	64 ms/projection						
Load cycles	1	2	3	4	5	6	7
Scan time (min)	2.3	4.5	6.8	9.0	11.3	13.5	15.8
Dose accumulated (kGy)	4.7	9.5	14.2	18.9	23.6	28.4	33.1

Values of the correlated bone volume, damaged bone volume and (mean and standard deviation) differential strain values from DVC are summarized in Table 2. The more irradiated specimen (32.9 kGy/tomogram) presented a decrease in the CV/BV as the number of load cycles increased (from 93.6% to 66.3%), consistent with the development of microcracks in the tissue. Conversely, the less irradiated specimen (4.7 kGy/tomogram) showed a more stable CV/BV for all the analysed images. The

application of Peirce's criterion concluded that the CV/BV after 4 and 6 cycles (lowest CV/BV) were outliers and strain results were therefore not computed. Mean and standard deviation of the differential strain values after the second loading cycle (first two consecutive tomograms) can be interpreted as indicators of the baseline strain uncertainties; these increase for lower exposure due to the decrease of image quality, with a precision value below 150  $\mu\epsilon$  for the highly-irradiated specimen and slightly above 500  $\mu\epsilon$  for the lowly-irradiated specimen. Both bone volume damage and differential strain value progressively increase with the applied loading cycles and consecutive scans. This increment was more dramatic in the 32.9 kGy specimen, with more than half its volume exceeding the considered threshold in the yield strain ( $\pm 10,000 \mu\epsilon$ ).

**Table 2.** Correlated bone volume (CV/BV), damaged bone volume (BV<sub>y</sub>) and mean  $\pm$  standard deviation of the differential strains ( $\Delta\epsilon$ ) for each loading cycle in the specimens subjected to highest (32.9 kGy/tomogram) and lowest (4.7 kGy/tomogram) radiation doses, as computed using DVC.

Dose/cycle	32.9 kGy					
Load cycles	2	3	4	5	6	7
CV/BV (%)	93.6	90.6	85.6	74.2	73.4	66.3
BV <sub>y</sub> (%)	0	0	0.24	30.1	61.2	57.1
$\Delta\epsilon$ ( $\mu\epsilon$ )	405 $\pm$ 142	828 $\pm$ 320	1546 $\pm$ 582	3632 $\pm$ 1660	5546 $\pm$ 2078	6752 $\pm$ 2830
Dose/cycle	4.7 kGy					
Load cycles	2	3	4	5	6	7
CB/BV (%)	94.3	88.5	72.7	88.4	73.7	88.3
BV <sub>y</sub> (%)	0	0	NC <sup>1</sup>	7.0	NC <sup>1</sup>	13.9
$\Delta\epsilon$ ( $\mu\epsilon$ )	928 $\pm$ 504	868 $\pm$ 502	NC <sup>1</sup>	1369 $\pm$ 1155	NC <sup>1</sup>	1563 $\pm$ 3142

<sup>1</sup> Not computed data. Data identified as outlier after applying the criterion of Peirce.

The internal differential strain distributions (first and third principal strain components) for the highly irradiated sample imaged are reported in Figure 6. The distribution of both components well described the damage events. After the first two loading cycles, the differential strain distribution was homogeneous throughout the entire volume (Fig. 6-I). As the loading cycles increased, the strain values increased, and the strain field became more heterogeneous (Fig. 6-II, III), in agreement with the random distribution of microcracks within the entire volume. The histograms for both differential principal strains (Fig. 6-IV) captured the strain evolution within the studied VOI. After two loading cycles, the number of sub-volumes exceeding  $\pm 1,000 \mu\epsilon$  was considerably low, however, increasing the loading cycles and therefore the total exposure to radiation, the number of sub-volumes exceeding those values increased significantly, reaching maximum amplitude values exceeding  $\pm 10,000 \mu\epsilon$  at the end of the test. In addition, a single trabecula was tracked during the different cycles to visualize the progression of strain coupled with the microdamage in the tissue (Fig. 7). It can be seen how maximum differential strains were reached in regions of microcracks development (red arrows). Microcracks location corresponded to strain values above 8,000  $\mu\epsilon$  in tension and 6,000  $\mu\epsilon$  in compression after 5 loading steps and exceeded  $\pm 10,000 \mu\epsilon$  at the end of the test. Despite the development of multiple microcracks, the overall look of the tracked trabecula did not present any noticeable change in the deformed configuration. Additionally, before damage became identifiable (5<sup>th</sup> cycle), the strain distribution seemed to predict the location of damage initiation. In an analogous manner, the differential strain distribution was plotted for the sample imaged at low radiation dose (4.7 kGy/tomogram). Both first and third

differential principal strains are shown in Figure 8. Although slightly higher strain values were found after loading the sample for seven cycles, the differences in the 3D full-field differential strains at the end of each step were minimal. The histograms (Fig. 8-IV) showed maximum amplitudes below 1,000  $\mu\epsilon$  in tension and compression after the 5<sup>th</sup> loading cycle and close to 3,000  $\mu\epsilon$  after the last loading step.

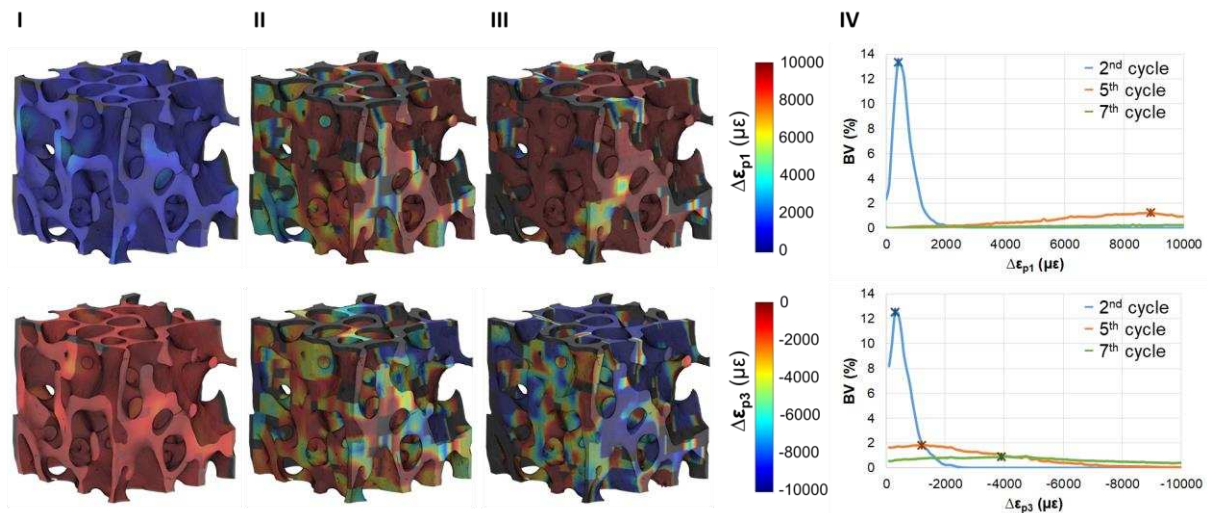


**Figure 6.** 3D differential strain distribution in trabecular bone tissue for the highly-irradiated sample (32.9 kGy/tomogram). First ( $\Delta\epsilon_{p1}$ ) and third ( $\Delta\epsilon_{p3}$ ) differential principal strains are represented after two (I), five (II) and seven (III) loading cycles. Histograms of the differential strain distribution in the tissue voxels (IV) after the same loading cycles are shown with the correspondent maximum strain amplitudes. High exposures produced an important damage in the bone during sequential tomograms and the differential first ( $\Delta\epsilon_{p1}$ ) and third ( $\Delta\epsilon_{p3}$ ) principal strains were largely above 10,000  $\mu\epsilon$  after the 7<sup>th</sup> cycle.

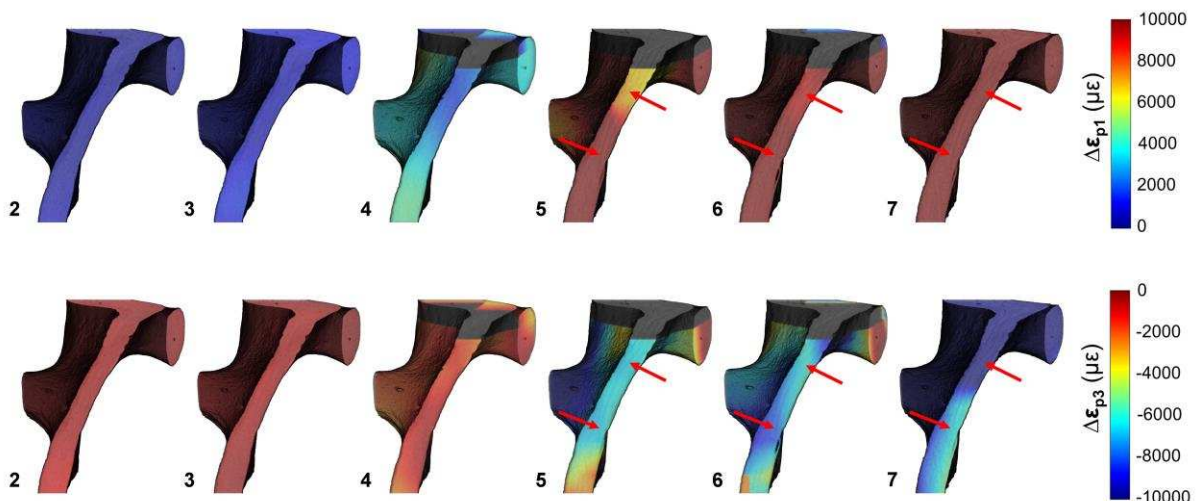


**Figure 7.** 3D distribution of first ( $\Delta\epsilon_{p1}$ ) and third ( $\Delta\epsilon_{p3}$ ) principal differential strains on a single trabecula tracked during the different loading cycles (cycle number indicated for each DVC computation) for the highly irradiated sample (32.9 kGy/tomogram). Arrows indicate microcracks visible in the tissue.

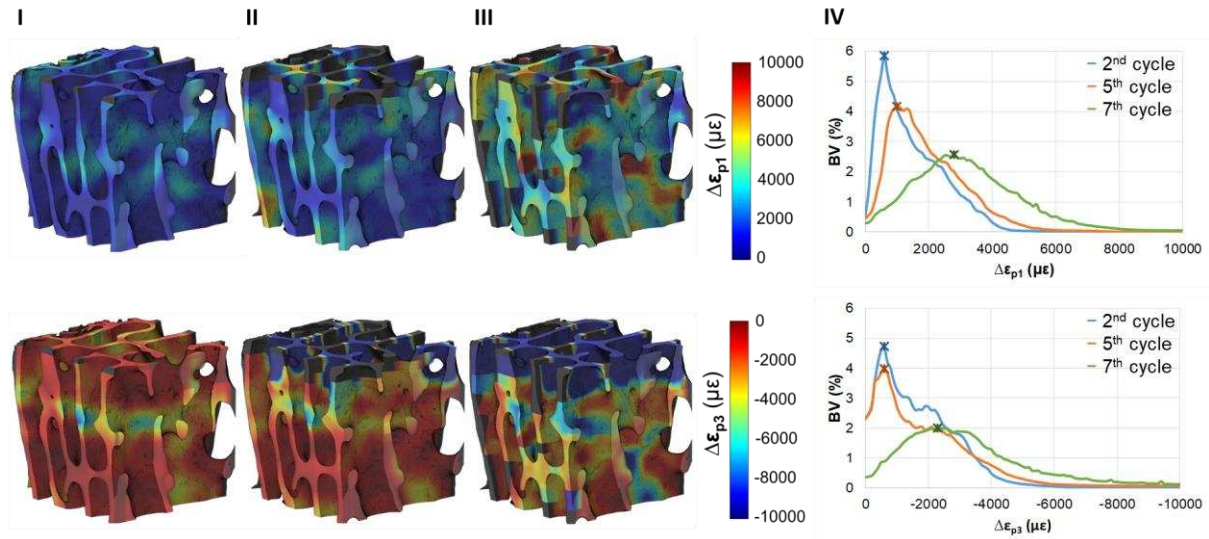


**Figure 8.** 3D differential strain distribution in trabecular bone tissue for the low-irradiated sample (4.7 kGy/tomogram). First ( $\Delta\epsilon_{p1}$ ) and third ( $\Delta\epsilon_{p3}$ ) differential principal strains are represented after two (I), five (II) and seven (III) loading cycles. Histograms of the differential strain distribution in the tissue voxels (IV) after the same loading cycles are shown with the correspondent maximum strain amplitudes. The reduction in exposure time considerably reduced the damage induced in the bone during sequential tomograms, although some areas of strain concentration could be identified.

#### 4. Discussion

The main aim of this paper was to investigate and quantify, for the first time, the influence of the irradiation-induced trabecular bone damage on its apparent elastic properties and local deformation using DVC applied to in situ SR-microCT images. Structurally, the irradiation affects the collagen environment (increasing the degree of cross-linking), resulting in a progressive loss in the post-yield deformation leading to a decline in strength, toughness and ductility of bone [16]; thus, special attention is needed for in situ mechanical studies involving high flux X-ray radiation. A deeper understanding of the full-field differential strain accumulated in the tissue due to the X-ray synchrotron radiation was achieved. In fact, despite that a number of studies used SR-microCT in conjunction with in situ mechanical testing to characterize bone microstructure and mechanics [13–15], the potential of DVC to high resolution SR-microCT remains partially unexplored [26,33].

The results reported in this paper clearly show the progressive strain accumulation in the tissue when increasing the total exposure time to SR X-ray radiation (Figs. 6, 7), and consequently the accumulated radiation dose. Furthermore, DVC successfully correlated the presence of microcracks in the highly-irradiated sample to large levels of tensile and compressive strains, above or close to the typical values of trabecular bone yielding (i.e. 6,200  $\mu\epsilon$  in tension and 10,400  $\mu\epsilon$  in compression [34] for human trabecular tissue and 7,800  $\mu\epsilon$  in tension and 10,900  $\mu\epsilon$  in compression [35] for bovine trabecular tissue). In fact, the main potential of DVC is in its ability to predict damage location before gross failure occurs, when high-strain concentrations typical of tissue yielding are building up [29,30]. In this sense, the results herein obtained clearly show how local strain concentration progressed from the 4<sup>th</sup> loading cycle and resulted in microcracks detection in the next cycle (Fig. 7). It could be argued that the applied repetitive loading during the experiment, much like a low cycle fatigue, may influence the full-field strain

measured in the tissue. In fact, it is not easy to decouple both phenomena. Singhal et al. [50] distinguished between the damage due to mechanical loading and irradiation by using control samples subjected only to load or irradiation and found that although the apparent modulus remained unaffected by both events, the residual strains were largely altered primarily due to the irradiation, and, to a lower extent, by mechanical loading. However, this type of analysis is not possible when using DVC applied to SR-microCT in situ tested samples, as image acquisition is needed, and this necessarily involves exposure to irradiation. Furthermore, for the less irradiated specimen (4.7 kGy/tomogram) some areas of strain concentration were identified using DVC from the second load cycle (Fig. 8) even though the apparent mechanical behaviour of such specimen was normal (Fig. 4-IV). This localised strain concentration was further recognised, and its evolution was tracked during the remaining loading steps. Despite the fact that all the specimens were loaded in the apparent elastic regime (0.5% global strain) and that the stress-strain curve for the 4.7 kGy specimen presented a linear elastic behaviour beyond 0.5% strain, some microstructural damage can still appear. In fact, as reported by Moore et al. [39] while an applied compressive strain of 0.4% resulted in no microdamage to the specimens, an increment of the strain from 0.4% to 0.8% showed an increase in the number of damaged trabeculae. Additionally, the top face of the specimen experienced important levels of compressive strain, more likely due to the applied load than to the radiation exposure. Also, as only a small VOI at the centre of the specimens was analysed it is then possible that strain concentration out of that region was not assessed using DVC, what may affect the computation on the edges of the VOI. However, the aim of this study was to quantify the effect of the irradiation on the bone tissue and it has been shown (Fig. 5) that maximum doses are accumulated in the centre of the specimen where the X-ray beam impinges. In order to define a safe exposure that would not compromise the mechanical stability of the tissues, different exposure times to SR irradiation were evaluated, leading to a wide range of radiation doses. The total radiation dose absorbed by the specimens depends on multiple factors (i.e. beam size, flux, energy, filters). However, the delivered dose rate is based on the specifications of the tomography beamlines (i.e. flux, energy) and it is more complex for users to control. Therefore, varying the total exposure time (number of projections and/or exposure per projection) results on a straightforward approach to achieve different radiation doses. In addition, being the current study based on DVC performance itself, it was decided to control exposure as for image quality. It has been shown (Fig. 3) that reducing the accumulated dose to 33 kGy facilitated tissue preservation, but at the same time the image quality was significantly reduced, as the exposure time was set to 64 ms/projection. This was perceived by DVC as important levels of strain uncertainties up to  $\sim 500 \mu\epsilon$ , although still acceptable to discriminate tissue yielding. Furthermore, the reduction of image quality may also be responsible for the low CV/BV found for the 4<sup>th</sup> and 6<sup>th</sup> loading cycles, identified as outliers. In any case, DVC indicated that the microdamage induced by irradiation was by far more important than the uncertainties (Figs. 6, 7). Two recent studies [33,47] measuring strain uncertainties on high-quality images obtained by SR-microCT reported SDER values below  $150 \mu\epsilon$  for an equivalent sub-volume size, close to the values obtained in this study for the highly irradiated specimen, where image quality is comparable. It is worth to recall that the strain uncertainties computed in this study were not based on a zero-strain test that is typically performed in DVC studies [33,44,46], as all the images were acquired under applied load and



this can potentially alter the significance of uncertainty measurement due to the random presence of mechanically accumulated strains. For this reason, all the registrations performed using DVC were considered as differential or residual strains, where the strain produced in the compression stage up to 0.5% could not be computed. In fact, since the aim of this work was to assess the effect of X-ray radiation on the apparent mechanics of the tissue, introducing two more scans before loading the specimens would have produced an additional dose accumulation on the specimens prior to the mechanical testing; hence, potentially altering the tissue properties. The reliability of DVC in terms of strain uncertainties on tissue measurements is limited in most microCT systems [44,51] that typically have low spatial resolution and SNR. By contrast, SR-microCT enables micro-resolution at high SNR, providing more features to improve DVC computation, and therefore the characterization in a 3D manner of bone microdamage. However, this study illustrates that when prolonged exposure times are required, the microstructural integrity of bone tissue is compromised. Consequently, one could question the results of any mechanical studies involving high irradiation levels. Hence, it is surprising that bone tissue behaviour has been previously studied using time-lapsed SR-microCT [14,26] and, although concerns about the effect of the irradiation were discussed, the possible microcracks formation and/or progression due to irradiation damage was never addressed.

The accumulated dose distribution delivered to each bone specimen was simulated using FLUKA Monte Carlo code, which has been extensively used for dose calculations in the medical field [52–54]. The simulation considered not only the trabecular bone specimen but also its environment, which seemed to considerably reduce the average dose rate compared to that of the bone in dry air (decrease on the average dose rate from 90 Gy/s in dry conditions (air) to 35 Gy/s in saline solution within the loading device). Bone specimens were simulated as homogeneous cylinders with an apparent density of 0.5 g/cm<sup>3</sup> (see supplementary material S2). The chosen density value is well aligned with the bone mineral density of ovine femoral condyles [55] and the average volume fraction ( $0.33 \pm 0.04$ ) of the four specimens, and in agreement with previous literature [43] on ovine trabecular bone. Despite a simulation based on the real trabecular geometry would be beneficial for a more accurate computation of the local dose accumulation in the tissue, it was not within the scope of this study to perform sample-specific dose simulations, but to have a close estimation on the absorbed dose. However, a correlation between tissue strain developed due to SR radiation and related local dose would be an attractive topic for further studies in the field.

The average dose computed in this study with FLUKA is well in agreement to that obtained using mathematical formulation previously proposed [16] (see supplementary material S2). Barth et al. [16] defined a “safe” irradiation level of 35 kGy and since then, this has been considered as a reference in several studies using SR radiation for imaging bone tissue [56,57]. That dose value corresponds to the maximum standard dose typically used in tissue banks in order to sterilize bone allografts for bone replacement [18]. In a follow-up study [17], it was suggested that no notable difference in the mechanical integrity of the bone could be detected for irradiation doses below 35 kGy. In agreement with that statement, the present study showed that for the less irradiated specimen (dose of ~33 kGy) the stress-strain curve presented a normal behaviour, although DVC identified higher strain values at the end of the loading cycles. High strains may as well be caused by localised tissue irradiation, other

than local mechanical strain concentration, which could not be visually detected in the reconstructed images due to the low SNR. In fact, the simulated dose rate can locally reach values of 60 Gy/s (Fig. 5), which results in a radiation dose of ~50 kGy for the less irradiated specimen after seven tomograms, and this may induce some tissue microdamage accumulated over sequential acquisition. This is an important aspect as some local microdamage could still be produced by SR radiation even when apparent average dose is contained within safe values. Additionally, it could be seen that for a total dose ~60 kGy, a loss of plasticity was observed for the 8.8 kGy/tomogram specimen (Fig. 4-V), in a comparable way as found by Barth et al. [16] for irradiation doses as low as 70 kGy. Most importantly, this study illustrates that the presence of microcracks is not always correlated with an alteration on the apparent mechanical properties of the bone (Fig. 3-I). In fact, despite the accumulated dose was above 230 kGy, the elastic apparent properties remained unaltered. This finding is particularly interesting and suggests how only apparent mechanical behaviour of bone is not necessarily indicative of structural integrity and preserved properties, when specimen is exposed to high-flux synchrotron radiation.

To date, different studies have investigated how SR radiation affects the deformation and fracture properties of human cortical bone [16,17] and bovine cortical bone [50], nevertheless this work presented the first quantification of the irradiation-induced damage at tissue level. At the apparent level, this study reported insignificant effect on the elastic behaviour; conversely, the plastic deformation was largely affected, in accordance to previous literature [16,17,50]. Strain evaluation on the irradiated specimens was carried out by Barth et al. [17] and Singhal et al. [50] using in situ Small- and Wide-Angle X-ray Scattering (SAXS and WAXS). A partition of strain between the collagen fibrils and mineral crystal is possible using both techniques; however, in situ SR-microCT overcome the limitations of two-dimensional information in SAXS and WAXS experiments, providing three-dimensional structural information. A correlation of different imaging techniques at various dimensional scales would allow a better understanding of the main mechanism causing the damage accumulation in the bone tissue. While SAXS and WAXS could provide information on the changes in the toughening at the level of the mineralized collagen fibrils and the mineral particles, in situ SR-microCT would allow visualization and quantification of the induced damage, as well as a full-field strain computation using DVC.

In situ SR-microCT mechanical testing and DVC require the acquisition of several tomograms to study deformation mechanisms. This process inevitably exposes the samples to higher SR radiation, sensitive in the case of biological tissues, and can vary depending on the proposed experimental design (i.e. number of in situ steps p/experiment). Synchrotron users could interact with beamline scientists ahead of the beamtime to evaluate the expected irradiation dose levels in advance and consequently plan the experiment based on the total amount of time that samples can be exposed.

However, further investigation should be performed to evaluate the optimal imaging setting preserving bone tissue integrity while maximizing imaging quality, and clearly establishing the damage induced on the tissue. In this way, DVC measured strain uncertainties could be minimised and successfully applied to SR-microCT in situ mechanically tested bone samples.

## 5. Conclusion

The internal full-field strain from DVC applied to SR-microCT images under a constant applied load at different cycling steps was measured in trabecular bone samples for different exposures to X-ray SR radiation. Local and average dose on the bone were simulated taking into account all the materials in the beam-path. Average maximum dose values ranged between ~33 and ~ 230 kGy for exposures of 64 and 512 ms per frame, respectively. Irradiation-induced microcracks developed in the tissue were successfully matched with important level of strain when a higher dose of 32.9 kGy/tomogram was used. Reduced exposure (64 ms/projection), leading to a considered safe average dose of 35 kGy, was able to control the microdamage and preserve the mechanical performance of the tissue, but notably decreased the quality of the images and consequently the DVC performance. Image settings and number of scans performed should be carefully chosen prior to any in situ SR-microCT experiment in order to maintain the radiation dose below the suggested safe threshold (35 kGy), without compromising the mechanical properties of the tissue. Future work is mandatory to clearly establish the damage induced on the tissue in SR-microCT for in situ mechanics, as well as consequent DVC performance.

## Acknowledgments

The authors would like to thank Diamond Light Source for time at the Diamond-Manchester Imaging Branchline I13-2 and the I13 Data Beamline [58] (proposal number MT14080), and the Zeiss Global Centre (University of Portsmouth) for post-processing. We further acknowledge Dr Dave Hollis (LaVision Ltd) for assistance with DaVis software and Dr Kazimir Wanelik for help during the experiment at Diamond Light Source.

## References

- [1] C.M.J. de Bakker, W.-J. Tseng, Y. Li, H. Zhao, X.S. Liu, Clinical Evaluation of Bone Strength and Fracture Risk, *Curr. Osteoporos. Rep.* 15 (2017) 32–42. doi:10.1007/s11914-017-0346-3.
- [2] M.A. Hammond, M.A. Gallant, D.B. Burr, J.M. Wallace, Nanoscale changes in collagen are reflected in physical and mechanical properties of bone at the microscale in diabetic rats, *Bone*. 60 (2014) 26–32. doi:10.1016/j.bone.2013.11.015.
- [3] A. Karunaratne, C.R. Esapa, J. Hiller, A. Boyde, R. Head, J.H.D. Bassett, N.J. Terrill, G.R. Williams, M.A. Brown, P.I. Croucher, S.D.M. Brown, R.D. Cox, A.H. Barber, R. V. Thakker, H.S. Gupta, Significant deterioration in nanomechanical quality occurs through incomplete extrafibrillar mineralization in rachitic bone: Evidence from in-situ synchrotron X-ray scattering and backscattered electron imaging, *J. Bone Miner. Res.* 27 (2012) 876–890. doi:10.1002/jbmr.1495.
- [4] M.L. Bouxsein, Bone quality: where do we go from here?, *Osteoporos. Int.* 14 (2003) 118–127. doi:10.1007/s00198-003-1489-x.
- [5] J.Y. Rho, L. Kuhn-Spearing, P. Zioupos, Mechanical properties and the hierarchical structure of bone, *Med. Eng. Phys.* 20 (1998) 92–102. doi:10.1016/S1350-4533(98)00007-1.
- [6] S. Ma, O. Boughton, A. Karunaratne, A. Jin, J. Cobb, U. Hansen, R. Abel, Synchrotron Imaging Assessment of Bone Quality, *Clin. Rev. Bone Miner. Metab.* 14 (2016) 150–160. doi:10.1007/s12018-016-9223-3.
- [7] S. Li, E. Demirci, V. V. Silberschmidt, Variability and anisotropy of mechanical behavior of cortical bone in tension and compression, *J. Mech. Behav. Biomed. Mater.* 21 (2013) 109–120. doi:10.1016/j.jmbbm.2013.02.021.
- [8] J.S. Nyman, H. Leng, X. Neil Dong, X. Wang, Differences in the mechanical behavior of cortical bone between compression and tension when subjected to progressive loading, *J. Mech. Behav. Biomed. Mater.* 2 (2009) 613–619. doi:10.1016/j.jmbbm.2008.11.008.
- [9] C. Öhman, M. Baleani, E. Perilli, E. Dall'Ara, S. Tassani, F. Baruffaldi, M. Viceconti, Mechanical testing of cancellous bone from the femoral head: Experimental errors due to off-axis

- measurements, *J. Biomech.* 40 (2007) 2426–2433. doi:10.1016/j.jbiomech.2006.11.020.
- [10] U. Wolfram, H.J. Wilke, P.K. Zysset, Damage accumulation in vertebral trabecular bone depends on loading mode and direction, *J. Biomech.* 44 (2011) 1164–1169. doi:10.1016/j.jbiomech.2011.01.018.
- [11] L. Babout, W. Ludwig, E. Maire, J.Y. Buffiere, J.Y. Buffi, Damage assessment in metallic structural materials using high resolution synchrotron X-ray tomography, *Nucl. Instruments Methods Phys. Res. Sect. B Beam Interact. with Mater. Atoms.* 200 (2003) 303–307. doi:10.1016/S0168-583X(02)01692-0.
- [12] J.A. Elliott, A.H. Windle, J.R. Hobdell, G. Eeckhaut, R.J. Oldman, W. Ludwig, E. Boller, P. Cloetens, J. Baruchel, In-situ deformation of an open-cell flexible polyurethane foam characterised by 3D computed microtomography, *J. Mater. Sci.* 37 (2002) 1547–1555. doi:10.1023/A:1014920902712.
- [13] R. Voide, P. Schneider, M. Stauber, P. Wyss, M. Stampanoni, U. Sennhauser, G.H. van Lenthe, R. Müller, Time-lapsed assessment of microcrack initiation and propagation in murine cortical bone at submicrometer resolution, *Bone.* 45 (2009) 164–173. doi:10.1016/j.bone.2009.04.248.
- [14] P.J. Thurner, P. Wyss, R. Voide, M. Stauber, M. Stampanoni, U. Sennhauser, R. Müller, Time-lapsed investigation of three-dimensional failure and damage accumulation in trabecular bone using synchrotron light, *Bone.* 39 (2006) 289–299. doi:10.1016/j.bone.2006.01.147.
- [15] A. Larrue, A. Rattner, N. Laroche, L. Vico, F. Peyrin, Feasibility of micro-crack detection in human trabecular bone images from 3D synchrotron microtomography, *Annu. Int. Conf. IEEE Eng. Med. Biol. - Proc.* (2007) 3918–3921. doi:10.1109/IEMBS.2007.4353190.
- [16] H.D. Barth, M.E. Launey, A.A. MacDowell, J.W. Ager, R.O. Ritchie, On the effect of X-ray irradiation on the deformation and fracture behavior of human cortical bone, *Bone.* 46 (2010) 1475–1485. doi:10.1016/j.bone.2010.02.025.
- [17] H.D. Barth, E.A. Zimmermann, E. Schaible, S.Y. Tang, T. Alliston, R.O. Ritchie, Characterization of the effects of x-ray irradiation on the hierarchical structure and mechanical properties of human cortical bone, *Biomaterials.* 32 (2011) 8892–8904. doi:10.1016/j.biomaterials.2011.08.013.
- [18] H. Nguyen, D.A.F. Morgan, M.R. Forwood, Sterilization of allograft bone: Effects of gamma irradiation on allograft biology and biomechanics, *Cell Tissue Bank.* 8 (2007) 93–105. doi:10.1007/s10561-006-9020-1.
- [19] J.Y. Buffiere, E. Maire, J. Adrien, J.P. Masse, E. Boller, In situ experiments with X ray tomography: An attractive tool for experimental mechanics, *Proc. Soc. Exp. Mech. Inc.* 67 (2010) 289–305. doi:10.1007/s11340-010-9333-7.
- [20] A. Nazarian, R. Müller, Time-lapsed microstructural imaging of bone failure behavior, *J. Biomech.* 37 (2004) 55–65. doi:10.1016/S0021-9290(03)00254-9.
- [21] B.K. Bay, T.S. Smith, D.P. Fyhrie, M. Saad, Digital volume correlation: Three-dimensional strain mapping using X-ray tomography, *Exp. Mech.* 39 (1999) 217–226. doi:10.1007/BF02323555.
- [22] L. Liu, E.F. Morgan, Accuracy and precision of digital volume correlation in quantifying displacements and strains in trabecular bone, *J. Biomech.* 40 (2007) 3516–3520. doi:10.1016/j.jbiomech.2007.04.019.
- [23] B.C. Roberts, E. Perilli, K.J. Reynolds, Application of the digital volume correlation technique for the measurement of displacement and strain fields in bone: A literature review, *J. Biomech.* 47 (2014) 923–934. doi:10.1016/j.jbiomech.2014.01.001.
- [24] F. Gillard, R. Boardman, M. Mavrogordato, D. Hollis, I. Sinclair, F. Pierron, M. Browne, The application of digital volume correlation (DVC) to study the microstructural behaviour of trabecular bone during compression, *J. Mech. Behav. Biomed. Mater.* 29 (2014) 480–499. doi:10.1016/j.jmbbm.2013.09.014.
- [25] E. Dall’Ara, D. Barber, M. Viceconti, About the inevitable compromise between spatial resolution and accuracy of strain measurement for bone tissue: A 3D zero-strain study, *J. Biomech.* 47 (2014) 2956–2963. doi:10.1016/j.jbiomech.2014.07.019.
- [26] D. Christen, A. Levchuk, S. Schori, P. Schneider, S.K. Boyd, R. Müller, Deformable image registration and 3D strain mapping for the quantitative assessment of cortical bone microdamage, *J. Mech. Behav. Biomed. Mater.* 8 (2012) 184–193. doi:10.1016/j.jmbbm.2011.12.009.
- [27] A.I. Hussein, Z.D. Mason, E.F. Morgan, Presence of intervertebral discs alters observed stiffness and failure mechanisms in the vertebra, *J. Biomech.* 46 (2013) 1683–1688. doi:10.1016/j.jbiomech.2013.04.004.
- [28] A.I. Hussein, P.E. Barbone, E.F. Morgan, Digital volume correlation for study of the mechanics of whole bones, *Procedia IUTAM.* 4 (2012) 116–125. doi:10.1016/j.piutam.2012.05.013.

- [29] V. Danesi, G. Tozzi, L. Cristofolini, Application of digital volume correlation to study the efficacy of prophylactic vertebral augmentation, *Clin. Biomech.* 39 (2016) 14–24. doi:10.1016/j.clinbiomech.2016.07.010.
- [30] G. Tozzi, V. Danesi, M. Palanca, L. Cristofolini, Elastic Full-Field Strain Analysis and Microdamage Progression in the Vertebral Body from Digital Volume Correlation, *Strain.* 52 (2016) 446–455. doi:10.1111/str.12202.
- [31] K. Madi, G. Tozzi, Q.H. Zhang, J. Tong, A. Cossey, A. Au, D. Hollis, F. Hild, Computation of full-field displacements in a scaffold implant using digital volume correlation and finite element analysis, *Med. Eng. Phys.* 35 (2013) 1298–1312. doi:10.1016/j.medengphy.2013.02.001.
- [32] G. Tozzi, Q.H. Zhang, J. Tong, Microdamage assessment of bone-cement interfaces under monotonic and cyclic compression, *J. Biomech.* 47 (2014) 3466–3474. doi:10.1016/j.jbiomech.2014.09.012.
- [33] M. Palanca, A.J. Bodey, M. Giorgi, M. Viceconti, D. Lacroix, L. Cristofolini, E. Dall'Ara, Local displacement and strain uncertainties in different bone types by digital volume correlation of synchrotron microtomograms, *J. Biomech.* c (2017). doi:10.1016/j.jbiomech.2017.04.007.
- [34] H.H. Bayraktar, E.F. Morgan, G.L. Niebur, G.E. Morris, E.K. Wong, T.M. Keaveny, Comparison of the elastic and yield properties of human femoral trabecular and cortical bone tissue, *J. Biomech.* 37 (2004) 27–35. doi:10.1016/S0021-9290(03)00257-4.
- [35] G.L. Niebur, M.J. Feldstein, J.C. Yuen, T.J. Chen, T.M. Keaveny, High-resolution finite element models with tissue strength asymmetry accurately predict failure of trabecular bone, *J. Biomech.* 33 (2000) 1575–1583. doi:10.1016/S0021-9290(00)00149-4.
- [36] T.M. Keaveny, R.E. Borchers, L.J. Gibson, W.C. Hayes, Theoretical analysis of the experimental artifact in trabecular bone compressive modulus, *J. Biomech.* 25 (1993) 599–607.
- [37] C. Rau, U. Wagner, Z. Pešić, A. De Fanis, Coherent imaging at the Diamond beamline I13, *Phys. Status Solidi Appl. Mater. Sci.* 208 (2011) 2522–2525. doi:10.1002/pssa.201184272.
- [38] R.C. Atwood, A.J. Bodey, S.W.T. Price, M. Basham, M. Drakopoulos, A high-throughput system for high-quality tomographic reconstruction of large datasets at Diamond Light Source, *Philos. Trans. R. Soc. A Math. Phys. Eng. Sci.* 373 (2015). doi:10.1098/rsta.2014.0398.
- [39] T.L.A. Moore, L.J. Gibson, Microdamage Accumulation in Bovine Trabecular Bone in Uniaxial Compression, *J. Biomech. Eng.* 124 (2002) 63. doi:10.1115/1.1428745.
- [40] M. Doube, M.M. Klosowski, I. Arganda-Carreras, F.P. Cordelières, R.P. Dougherty, J.S. Jackson, B. Schmid, J.R. Hutchinson, S.J. Shefelbine, BoneJ: Free and extensible bone image analysis in ImageJ, *Bone.* 47 (2010) 1076–1079. doi:10.1016/j.bone.2010.08.023.
- [41] T. Tanaka, H. Kitamura, SPECTRA: A synchrotron radiation calculation code, *J. Synchrotron Radiat.* 8 (2001) 1221–1228. doi:10.1107/S090904950101425X.
- [42] G. Battistoni, F. Cerutti, A. Fassò, A. Ferrari, S. Muraro, J. Ranft, S. Roesler, P.R. Sala, The FLUKA code: Description and benchmarking, *AIP Conf. Proc.* 896 (2007) 31–49. doi:10.1063/1.2720455.
- [43] A. Nafei, C.C. Danielsen, A. Odgaard, F. Linde, I. Hvid, Properties of growing trabecular ovine bone. Part I: mechanical and physical properties., *J. Bone Joint Surg. Br.* 82 (2000) 910–920.
- [44] M. Palanca, G. Tozzi, L. Cristofolini, M. Viceconti, E. Dall'Ara, 3D Local Measurements of Bone Strain and Displacement: Comparison of Three Digital Volume Correlation Approaches., *J. Biomech. Eng.* 137 (2015) 1–14. doi:10.1115/1.4030174.
- [45] G. Tozzi, Q.H. Zhang, J. Tong, 3D real-time micromechanical compressive behaviour of bone-cement interface: Experimental and finite element studies, *J. Biomech.* 45 (2012) 356–363. doi:10.1016/j.jbiomech.2011.10.011.
- [46] G. Tozzi, E. Dall, M. Palanca, M. Curto, F. Innocente, L. Cristofolini, Journal of the Mechanical Behavior of Biomedical Materials Strain uncertainties from two digital volume correlation approaches in prophylactically augmented vertebrae : Local analysis on bone and cement- bone microstructures, *J. Mech. Behav. Biomed. Mater.* 67 (2017) 117–126. doi:10.1016/j.jmbbm.2016.12.006.
- [47] E. Dall'Ara, M. Peña-Fernández, M. Palanca, M. Giorgi, L. Cristofolini, G. Tozzi, Precision of DVC approaches for strain analysis in bone imaged with  $\mu$ CT at different dimensional levels, *Front. Mater.* 4:31 (2017). doi:10.3389/fmats.2017.00031.
- [48] M. Palanca, L. Cristofolini, E. Dall'Ara, M. Curto, F. Innocente, V. Danesi, G. Tozzi, Digital volume correlation can be used to estimate local strains in natural and augmented vertebrae: an organ-level study, *J. Biomech.* 49 (2016) 3882–3890. doi:10.1016/j.jbiomech.2016.10.018.
- [49] S.M. Ross, Peirce's criterion for the elimination of suspect experimental data, *J. Eng. Technol.* 20 (2003) 1–12. <http://classes.engineering.wustl.edu/2009/fall/che473/handouts/OutlierRejection.pdf>.

- [50] A. Singhal, A.C. Deymier-Black, J.D. Almer, D.C. Dunand, Effect of high-energy X-ray doses on bone elastic properties and residual strains, *J. Mech. Behav. Biomed. Mater.* 4 (2011) 1774–1786. doi:10.1016/j.jmbbm.2011.05.035.
- [51] L. Grassi, H. Isaksson, Extracting accurate strain measurements in bone mechanics: A critical review of current methods, *J. Mech. Behav. Biomed. Mater.* 50 (2015) 43–54. doi:10.1016/j.jmbbm.2015.06.006.
- [52] T.T. Böhlen, F. Cerutti, M.P.W. Chin, A. Fassò, A. Ferrari, P.G. Ortega, A. Mairani, P.R. Sala, G. Smirnov, V. Vlachoudis, The FLUKA Code: Developments and challenges for high energy and medical applications, *Nucl. Data Sheets.* 120 (2014) 211–214. doi:10.1016/j.nds.2014.07.049.
- [53] F. Botta, A. Mairani, R.F. Hobbs, A. Vergara Gil, M. Pacilio, K. Parodi, M. Cremonesi, M.A. Coca Pérez, A. Di Dia, M. Ferrari, F. Guerriero, G. Battistoni, G. Pedroli, G. Paganelli, L.A. Torres Aroche, G. Sgouros, Use of the FLUKA Monte Carlo code for 3D patient-specific dosimetry on PET-CT and SPECT-CT images., *Phys. Med. Biol.* 58 (2013) 8099–120. doi:10.1088/0031-9155/58/22/8099.
- [54] K. Parodi, A. Ferrari, F. Sommerer, H. Paganetti, Clinical CT-based calculations of dose and positron emitter distributions in proton therapy using the FLUKA Monte Carlo code, *Phys. Med. Biol.* 52 (2007) 3369–3387. doi:10.1088/0031-9155/52/12/004.
- [55] Z. Wu, W. Lei, Y. Hu, H. Wang, S. Wan, Z. Ma, H. Sang, S. Fu, Y. Han, Effect of ovariectomy on BMD, micro-architecture and biomechanics of cortical and cancellous bones in a sheep model, *Med. Eng. Phys.* 30 (2008) 1112–1118. doi:10.1016/j.medengphy.2008.01.007.
- [56] A. Karunaratne, L. Xi, L. Bentley, D. Sykes, A. Boyde, C.T. Esapa, N.J. Terrill, S.D.M. Brown, R.D. Cox, R. V. Thakker, H.S. Gupta, Multiscale alterations in bone matrix quality increased fragility in steroid induced osteoporosis, *Bone.* 84 (2016) 15–24. doi:10.1016/j.bone.2015.11.019.
- [57] S. Ma, E.L. Goh, A. Jin, R. Bhattacharya, O.R. Boughton, B. Patel, A. Karunaratne, N.T. Vo, R. Atwood, J.P. Cobb, U. Hansen, R.L. Abel, Long-term effects of bisphosphonate therapy: perforations, microcracks and mechanical properties, *Nat. Publ. Gr.* (2017) 1–10. doi:10.1038/srep43399.
- [58] A.J. Bodey, C. Rau, Launch of the I13-2 data beamline at the Diamond Light Source synchrotron, *J. Phys. Conf. Ser.* 849 (2017). doi:10.1088/1742-6596/849/1/012038.